Lattice Green function for extended defect calculations: Computation and error estimation with long-range forces

D. R. Trinkle*
Materials and Manufacturing Directorate, Air Force Research Laboratory, Wright Patterson Air Force Base, Dayton, Ohio 45433-7817, USA
(Received 29 May 2008; published 23 July 2008)

Computing the atomic geometry of lattice defects—e.g., point defects, dislocations, crack tips, surfaces, or boundaries—requires an accurate coupling of the local deformations to the long-range elastic field. Periodic or fixed boundary conditions used by classical potentials or density-functional theory may not accurately reproduce the correct bulk response to an isolated defect; this is especially true for dislocations. Flexible boundary conditions have been developed to produce the correct long-range strain field from a defect—effectively "embedding" a finite-sized defect with infinite bulk response, isolating it from either periodic images or free surfaces. Flexible boundary conditions require the calculation of the bulk response with the lattice Green function (LGF). While the LGF can be computed from the force-constant matrix, the force-constant matrix is only known to a maximum range. This paper illustrates how to accurately calculate the lattice Green function and estimate the error using a truncated force-constant matrix combined with knowledge of the long-range behavior of the lattice Green function. The effective range of deviation of the lattice Green function from the long-range elastic behavior provides an important length scale in multiscale quasicontinuum and flexible boundary-condition calculations, and measures the error introduced with periodic-boundary conditions.

DOI: 10.1103/PhysRevB.78.014110 PACS number(s): 61.72.Bb, 61.72.J−, 61.72.Lk, 61.72.Mm

I. INTRODUCTION

Lattice defects—e.g., interstitials, vacancies, dislocations, crack tips, free surfaces, interfaces, and boundaries—each play key roles in material properties[1] and, in order to understand defects, one must know their geometry. The far-field geometry for many defects is accurately described by anisotropic elasticity theory.[2,3] However, the elastic solution often diverges near the atomic-scale center of the defect and, in many cases, the center is difficult to investigate with current microscopy techniques. This is especially true of dislocations, which control plasticity in metals[1] and can severely limit device utility in semiconductors.[4] Only recently has the geometry and electronic structure of an isolated dislocation been calculated[5–7] despite the rapid advances in computer hardware and density-functional theory methods. Previous density-functional theory calculations were limited by the long-range strain field of a dislocation, which is incommensurate with periodic-boundary conditions; hence, only dislocation dipoles[8,9] or quadrupoles[10,11] had been computed. The advent of "flexible" or "Green function" boundary conditions—first conceived by Sinclair *et al.*,[12] later redeveloped for crack propagation,[13] and for dislocations and dislocation kinks[14]—made possible the relaxation of the core geometry of an isolated dislocation. For a review of density-functional theory methods applied to dislocations, see Ref. 15. Flexible boundary conditions accurately treat the long-range strain field away from the defect by using the harmonic ideal lattice response in the form of the lattice Green function (LGF). The lattice Green function determines the relaxed position of an atom, given the force on it and its neighbors in infinite bulk. Flexible boundary conditions have been used to model cracks,[13,16] dislocations, and kinks in bcc metals with classical potentials,[17,18] cross-slip processes in fcc metals,[19] isolated screw dislocations in bcc metals and ordered intermetallics with density-functional theory,[5–7] and even vacancies and free surfaces;[20] for a review of flexible boundary-condition approaches to nanomechanics of defects, see Ref. 21.

Flexible boundary conditions use the perfect lattice Green function to relax the forces on atoms near a defect by coupling to an infinite bulk; in this way, simulation of a defect requires only a small number of atoms near the defect geometry while the lattice Green function determines the displacement of bulklike atoms away from the defect. The lattice Green function $\underline{G}^L(\vec{R}-\vec{R}')$ gives displacements in response to the Kanzaki forces near the defect,

$$\vec{u}(\vec{R}') = -\sum_{\vec{R}} \underline{G}^L(\vec{R}-\vec{R}')\vec{f}(\vec{R}),$$

in the harmonic limit.[12,14] This gives an accurate treatment of the long-range stress field of a defect (such as a dislocation) while using density-functional theory forces close to the defect. Since the perfect lattice Green function has translational symmetry, it provides the "flexibility" in flexible boundary conditions: bulk lattice response is simulated *without* specifying an origin for the lattice. Moreover, using density-functional theory for the forces and the lattice Green function ensures accurate coupling of the defect region to infinite bulk without the mismatch of coupling classical potentials with density-functional theory.

Flexible boundary conditions are limited by the accuracy of the lattice Green function. Many closed-form results are known for the lattice Green functions of cubic lattices with nearest-neighbor interactions.[22,23] While the lattice Green function is intimately related to the elastic constants and force-constant matrix of a crystal, it has previously been computed for realistic potentials from relaxation of atom positions given an applied force.[12] Rao *et al.*[14] employed a

"direct displacement" technique where separate relaxation calculations in a two-dimensional (2D) slab are used to numerically evaluate the lattice Green function for short range while switching to the known long-range behavior of the elastic Green function (EGF). Woodward and Rao[5] used this same technique with density-functional theory for Mo, Ta, and TiAl, and found the lattice Green function matched the long-range behavior at distances of only 5 Å despite long-range metallic bonding. However, this technique is dependent on the defect geometry: a lattice Green function computed for a $[110]/2$ fcc screw dislocation cannot be used for the fcc edge dislocation with a threading direction of $[1\bar{1}2]/2$. Moreover, relying on atomic relaxation can be prone to error in density-functional methods when the applied forces become small. An accurate and computationally efficient approach instead relies on the force-constant matrix and elastic constants, which can be computed using standard techniques.

What follows is a general and accurate method for the computation of the lattice Green function applicable for use in density-functional theory for a variety of defect geometries. In addition, this paper presents and tests an estimate of the error in the lattice Green function due to the geometry limitations of periodic-boundary conditions with density-functional theory. Currently available methods for computing the force-constant matrix in density-functional theory effectively produce a truncated force-constant matrix, defined out to an artificial cutoff whether they rely on a finite supercell or calculated on a discrete k-point grid.[24–29] However, the interactions in density-functional theory have an unknown range, likely to be larger than the artificial supercell. Computing the lattice Green function requires (1) a computational algorithm to accurately use the limited force-constant matrix information and (2) an estimate of the error introduced from the force-constant matrix limitation.

Section II reviews the lattice harmonic response functions—the force constant and dynamical matrices, and lattice Green function—and relation to continuum elasticity theory. Section III derives the general procedure for accurate numerical evaluation of the lattice Green function with specific application for zero-dimensional (0D), one-dimensional (1D), and two-dimensional (2D) defects—point defects, dislocations, and boundaries, respectively. Section IV derives an error estimate for the lattice Green function using only the force-constant matrix computation from a *single* supercell and elastic constants. The error estimate is numerically tested using a face-centered-cubic lattice with random long-range interactions and is shown to be accurate even with supercells far smaller than the interaction range. Finally, Sec. V concludes with discussion of applications to defect calculations and the inherent length-scales in quasicontinuum methods used in multiscale applications.

II. HARMONIC LATTICE RESPONSE

When atoms in a crystal are subject to applied or internal forces, they respond by displacing from their ideal lattice sites, and conversely, displacement from the ideal lattice sites produces internal forces on atoms. For small displacements and forces, atoms respond harmonically with a linear relationship between displacement and force, given by two different lattice functions: the force-constant matrix/dynamical matrix, and lattice Green function. These functions are defined and connected to anisotropic elasticity. For simplicity, a single-atom basis Bravais lattice is assumed; ionic crystals have additional complexities that are not addressed here.[41]

The infinite harmonic crystal is well known from classical and quantum theory.[30,31] For lattice sites $\vec{R}$ and $\vec{R}'$, the 3×3 force-constant matrix $\underline{D}(\vec{R}-\vec{R}')$ determines the force at $\vec{R}$ from displacements at $\vec{R}'$, where

$$\underline{D}_{ab}(\vec{R}-\vec{R}') = \left.\frac{\partial^2 U^{\text{total}}}{\partial u_a(\vec{R})\,\partial u_b(\vec{R}')}\right|_{\vec{u}=\mathbf{0}}.$$

In addition to translational symmetry, $\underline{D}_{ab}(\vec{R})=\underline{D}_{ab}(-\vec{R})=\underline{D}_{ab}(\vec{R})$ due to inversion symmetry and independence of differentiation order, and obeys the sum rule $\Sigma_{\vec{R}}\underline{D}(\vec{R})=\mathbf{0}$. The method of long waves[30] connects the force-constant matrix and the elastic constants C_{abcd},

$$-\sum_{\vec{R}} \underline{D}_{ab}(\vec{R})R_cR_d = V(C_{acbd}+C_{adbc}), \tag{1}$$

where V is the volume of the unit cell. The static lattice Green function $\underline{G}^L(\vec{R}-\vec{R}')$ determines the displacement at $\vec{R}$ in response to a force at $\vec{R}'$; it obeys similar symmetries to the force-constant matrix: $\underline{G}^L_{ab}(\vec{R})=\underline{G}^L_{ab}(-\vec{R})=\underline{G}^L_{ab}(\vec{R})$. The long-range behavior of the lattice Green function is given by the elastic Green function from continuum theory. The elastic Green function $\underline{G}^E(\vec{x})$ satisfies the partial differential equation[2,3]

$$\sum_{abc} C_{iabc}\nabla_a\nabla_b\underline{G}^E_{cj}(\vec{x}) = -\delta_{ij}\delta(\vec{x}), \tag{2}$$

where $\delta(\vec{x})$ is the Dirac delta function. The lattice Green function matches the elastic Green function as $\vec{R}\to\infty$, regardless of how long ranged the force-constant matrix is. Lastly, the lattice Green function and force-constant matrix are (pseudo)inverses of each other,

$$\sum_{\vec{R}''} \underline{D}(\vec{R}-\vec{R}'')\underline{G}^L(\vec{R}''-\vec{R}') = \mathbf{1}\delta(\vec{R}-\vec{R}'), \tag{3}$$

where δ is the Kronecker delta function. The force-constant matrix is singular due to the sum rule and hence cannot be directly inverted with Eq. (3) to compute the lattice Green function.

The lattice Green function can be modified for different bulk boundary conditions. In infinite bulk, $\underline{G}^L$ is called the three-dimensional (3D) lattice Green function and it is useful for computation of point defects. If the forces and displacements have periodicity along a lattice vector $\vec{t}$, such as in a single straight dislocation defect, the 2D lattice Green function is used: $\Sigma_n\underline{G}^L(\vec{R}+n\vec{t})$. Finally, if forces and displacements have periodicity along two lattice vectors $\vec{t}_1$ and $\vec{t}_2$, such as in surfaces, grain boundaries, and interfaces, the 1D

lattice Green function is used: $\Sigma_{mn}\underline{G}^L(\vec{R}+m\vec{t}_1+n\vec{t}_2)$. Despite the simple summations used to define the 2D and 1D lattice Green functions from the 3D, the sums converge conditionally. The "dimensionality" of the lattice Green functions refer to the degrees of freedom for the lattice vector $\vec{R}$; $\underline{G}^L$ remains a 3×3 matrix in all cases. The dimensionality of the defect (0, 1, or 2) plus the dimensionality of the lattice Green function (3, 2, or 1) sums to three.

The computation of the lattice Green function is more tractable in reciprocal space. The lattice functions can be written as periodic functions of vectors $\vec{k}$ in the Brillouin zone (BZ) of reciprocal space,[32]

$$\tilde{G}^L(\vec{k}) = \sum_{\vec{R}} e^{i\vec{k}\cdot\vec{R}}\underline{G}^L(\vec{R}),$$

$$\underline{G}^L(\vec{R}) = V\int\int\int_{\mathrm{BZ}} \frac{d^3k}{(2\pi)^3} e^{-i\vec{k}\cdot\vec{R}}\tilde{G}^L(\vec{k}),$$

and a similar relationship between the force-constant matrix $\underline{D}$ and the dynamical matrix $\tilde{D}$. In reciprocal space, the inverse equation Eq. (3) simplifies to $\tilde{G}^L(\vec{k})\tilde{D}(\vec{k})=\mathbf{1}$ for all $\vec{k}$. The singularity of $\underline{D}$ is reduced to the gamma point $\vec{k}=0$, where $\tilde{D}(0)=\mathbf{0}$; for all other points, $\tilde{G}^L(\vec{k})=[\tilde{D}(\vec{k})]^{-1}$. The inverse exists for crystal structures without unstable phonon modes. The acoustic modes in the dynamical matrix produce a second-order pole in $\tilde{G}^L$ at the gamma point; this pole corresponds to the elastic Green function.

Accurate computation of lattice Green function relies on accurate computation of the force-constant matrix. While computing the force-constant matrix is straightforward for interactions with a finite cutoff, it is difficult for density-functional theory methods, which may have long-range interactions (such as Friedel oscillations). Two methods have emerged: direct force[24–27] and linear response.[28,29] The direct force method computes the reciprocal-space dynamical matrix on a discrete grid of k points in the BZ; this is equivalent to folding the force-constant matrix into an artificial supercell. Linear response can be used to compute the dynamical matrix at any arbitrary k point; however, finite computational time means that it, too, can only compute the dynamical matrix for a finite set of k points.

The effect of using a spatially truncated force-constant matrix to compute the lattice Green function needs to be evaluated. This is done with the elastic constants, which can be found separately by computing the response of a periodic cell to uniform strains. Equation (1) relates the elastic constants to the force-constant matrix. This provides an estimate for the deviation of the long-range elastic Green function from the lattice Green function, which in turn gives an error estimate for using the truncated force-constant matrix. More importantly, this estimate does not rely on a convergence test computation comparing increasingly larger supercells.

III. COMPUTATION OF LATTICE GREEN FUNCTION

The procedure for numerical computation of the lattice Green function in real space separates the Fourier transform into pieces, which can be inverse Fourier transformed accurately. The straightforward approach would be to discrete inverse Fourier transform the inverse of the dynamical matrix; however, this transform converges very slowly with increased grid spacing due to the second-order pole at the gamma point. The inversion of the dynamical matrix to compute the lattice Green function is still best performed in reciprocal space where the large R behavior is exactly contained in the pole at $k=0$. To accurately compute the lattice Green function requires an analytic treatment of the small k behavior separated from the rest of the Brillouin zone.

The separation of the lattice Green function allows a discrete inverse Fourier transform to converge by analytically treating the second-order pole and discontinuity at $k=0$. The second-order pole and discontinuity in $\tilde{G}^L$ comes from the expansion of $\tilde{D}(\vec{k})$ for small k,

$$\tilde{D}(\vec{k}) = \sum_{\vec{R}} \underline{D}(\vec{R})\exp(i\vec{k}\cdot\vec{R}) \approx \sum_{\vec{R}} \underline{D}(\vec{R})\left[1-\frac{1}{2}(\vec{k}\cdot\vec{R})^2+\frac{1}{24}(\vec{k}\cdot\vec{R})^4\right]. \quad (4)$$

The expansion is rewritten in terms of two functions of different order in k: $k^2\tilde{\Lambda}^{(2)}(\hat{k})-k^4\tilde{\Lambda}^{(4)}(\hat{k})$, where $\hat{k}=\vec{k}/k$. The first function $\tilde{\Lambda}^{(2)}(\hat{k})$ relates to the elastic constants by Eq. (1),

$$\sum_{cd} k_c k_d\left\{-\frac{1}{2}\sum_{\vec{R}} \underline{D}_{ab}(\vec{R})R_cR_d\right\} = V\sum_{cd} k_c C_{cabd}k_d,$$

which gives $\tilde{\Lambda}^{(2)}(\hat{k})=V[\hat{k}\mathbf{C}\hat{k}]$, where $\mathbf{C}$ is the fourth-rank elastic stiffness tensor. The quartic function $\tilde{\Lambda}^{(4)}(\hat{k})$ is

$$\tilde{\Lambda}^{(4)}(\vec{k}) = \sum_{cdef} k_c k_d k_e k_f\left\{-\frac{1}{24}\sum_{\vec{R}} \underline{D}(\vec{R})R_cR_dR_eR_f\right\}.$$

The lattice Green function expands for small k as

$$\tilde{G}^L(\vec{k}) = k^{-2}[\tilde{\Lambda}^{(2)}(\hat{k})]^{-1} + k^0[\tilde{\Lambda}^{(2)}(\hat{k})]^{-1}\tilde{\Lambda}^{(4)}(\hat{k})[\tilde{\Lambda}^{(2)}(\hat{k})]^{-1} + O(k^2),$$

where

$$\tilde{G}^E(\vec{k}) \equiv k^{-2}[\tilde{\Lambda}^{(2)}(\hat{k})]^{-1} = \frac{1}{Vk^2}[\hat{k}\mathbf{C}\hat{k}]^{-1}, \quad (5)$$

and

$$\tilde{G}^{\mathrm{dc}}(\vec{k}) \equiv [\tilde{\Lambda}^{(2)}(\hat{k})]^{-1}\tilde{\Lambda}^{(4)}(\hat{k})[\tilde{\Lambda}^{(2)}(\hat{k})]^{-1} = \tilde{G}^{\mathrm{E}}(\hat{k})\left[-\frac{1}{24}\sum_{\vec{R}} \underline{D}(\vec{R})(\hat{k}\cdot\vec{R})^4\right]\tilde{G}^E(\hat{k}). \quad (6)$$

$\tilde{G}^E$ is the second-order pole at the gamma point, which is the Fourier transform of the elastic Green function, while $\tilde{G}^{\mathrm{dc}}$ depends only on $\hat{k}$, gives a discontinuity at the gamma point [$\lim_{\vec{k}\to0}\tilde{G}^{\mathrm{dc}}(\vec{k})$ does not exist]. It is important to note that after subtracting the elastic Green function from the lattice Green function, a discontinuity is produced at the gamma

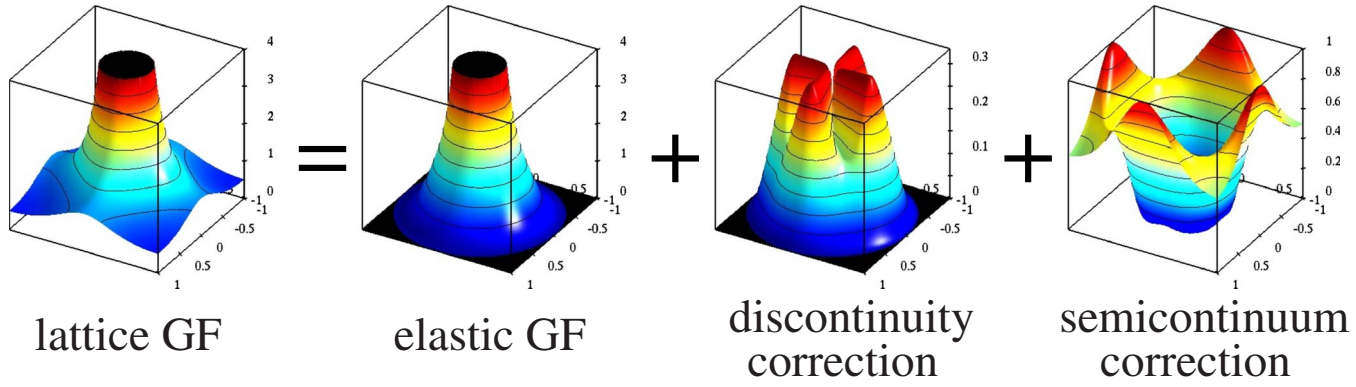

FIG. 1. (Color online) Separation of lattice Green function for a square lattice in two-dimensional reciprocal space into elastic Green function, discontinuity correction, and semicontinuum function (note different vertical scales). The lattice Green function has the periodicity of the reciprocal lattice and a second-order pole at the gamma point. The elastic Green function scales as k^{-2} and is cut off to smoothly go to zero at the Brillouin-zone edges. The removal of the second-order pole creates a discontinuity independent of $|k|$ at the gamma point; the discontinuity correction removes the discontinuity and smoothly goes to zero at the Brillouin-zone edges. The remaining difference between the lattice Green function and the first two terms is the semicontinuum function, which is smooth everywhere in the Brillouin zone.

point, which, if not handled before using a discrete inverse Fourier transform, will lead to slow convergence (albeit not as slow as the pole).

This expansion is used to rewrite the Fourier transform of the lattice Green function in the entire Brillouin zone as three pieces to be inverse Fourier transformed: the elastic Green function, discontinuity correction, and semicontinuum function. Truncating the elastic Green function and discontinuity correction relies on a continuous and differentiable cut-off function $f_{\text{cut}}(k/k_{\max})$ with parameter $0<\alpha<1$,

$$f_{\text{cut}}(x)=\begin{cases}1 & :0\le x<\alpha\\ 3\left(\dfrac{1-x}{1-\alpha}\right)^2-2\left(\dfrac{1-x}{1-\alpha}\right)^3 & :\alpha\le x<1\\ 0 & :1\le x\end{cases}, \quad (7)$$

where $k_{\max}$ is the radius of a sphere inscribed in the Brillouin zone. While the evaluation of $\underline{G}^L(\vec{R})$ is independent of the cut-off function, and hence α, the results shown use $\alpha=1/2$. Then, the lattice Green function for $\vec{k}$ in the first Brillouin zone is

$$\tilde{G}^L(\vec{k})=\tilde{G}^E(\vec{k})f_{\text{cut}}(k/k_{\max})+\tilde{G}^{\text{dc}}(\vec{k})f_{\text{cut}}(k/k_{\max})+\{[\tilde{D}(\vec{k})]^{-1}-[\tilde{G}^E(\vec{k})+\tilde{G}^{\text{dc}}(\vec{k})]f_{\text{cut}}(k/k_{\max})\}. \quad (8)$$

The term in braces is the semicontinuum function $\tilde{G}^{\text{sc}}$. It is the only function that is inverse Fourier transformed using a discrete numerical mesh; the elastic Green function and discontinuity are handled analytically. The elimination of the second-order pole at the gamma point by using a cut-off version of the elastic Green function is related to the semicontinuum method of Tewary and Bullough.[33] However, their semicontinuum approach used a Gaussian cutoff, which does not vanish at the Brillouin-zone edge and does not treat the discontinuity produced at the gamma point. Expressions using a Gaussian cutoff are included in the online supporting material.[42]

Figure 1 shows an example of the separation from Eq. (8) of the lattice Green function into the three terms for a square lattice. The lattice Green function shown comes from a square lattice with lattice constant $a_0=\pi$ and nearest-neighbor interactions; then $\tilde{G}^L(k_x,k_y)=[\sin^2(\pi k_x/2)+\sin^2(\pi k_y/2)]^{-1}$. The second-order pole at origin is given by the elastic Green function $\tilde{G}^E(k_x,k_y)=4/(\pi|k|)^2$; it is multiplied by the cut-off function with $k_{\max}=1$ so as to vanish at the Brillouin-zone edge. Subtracting the pole from the lattice Green function produces a function with a discontinuity at the gamma point. The discontinuity at the origin is given by the discontinuity correction $\tilde{G}^{\text{dc}}(k_x,k_y)=(k_x^4+k_y^4)/(3|k|^4)$, which is multiplied by the cut-off function. Note, e.g., that $\lim_{k\to 0}\tilde{G}^{\text{dc}}(k,0)=\frac{1}{3}\neq\lim_{k\to 0}\tilde{G}^{\text{dc}}(\sqrt{2}k,\sqrt{2}k)=\frac{1}{6}$, and this discontinuity only appears after removing the second-order pole. Subtracting the discontinuity produces the semicontinuum function, $\tilde{G}^{\text{sc}}(k_x,k_y)$, given by Eq. (8).

The evaluation of the lattice Green function in real space is accomplished by inverse Fourier transforming the semicontinuum function $\tilde{G}^{\text{sc}}$, the cut-off elastic Green function $\tilde{G}^E f_{\text{cut}}$, and the cut-off discontinuity correction $\tilde{G}^{\text{dc}} f_{\text{cut}}$. The semicontinuum function $\tilde{G}^{\text{sc}}(\vec{k})$ is evaluated on a discrete k-point grid in the Brillouin zone; inversion of the dynamical matrix for small k must be handled carefully to avoid numerical noise. A discrete inverse Fourier transform converges well with grid spacing because $\tilde{G}^{\text{sc}}$ is smooth throughout the Brillouin zone. The cut-off elastic Green function $\tilde{G}^E f_{\text{cut}}$ and discontinuity correction $\tilde{G}^{\text{dc}} f_{\text{cut}}$ are expanded as functions of $\hat{k}$ using spherical harmonics or a Fourier series depending on the dimensionality of the problem. In this form, their inverse Fourier transforms can be analytically reduced to a one-dimensional integral of nonsingular functions over a finite range that is computed numerically to the desired accuracy. The details of this reduction depends on the periodicity of the lattice Green function. Table I gives a brief overview of the results and Table II gives a summary of the equations; the online supporting material contains full derivations of the final expressions.[42]

TABLE I. Overview of lattice Green function computation for different dimensionality. The dimensionality of the lattice Green function is determined by the type of defect being simulated: the defect dimensionality plus the lattice Green function dimensionality is three. While the lattice Green function has the same form in reciprocal space, the periodicity determines the range of Brillouin-zone integration, and the functions used to expand the $\hat{k}$ dependence of the elastic Green function and discontinuity correction. The range of BZ integration produces different large R behavior for both the elastic Green function—also given by elasticity theory—and the discontinuity correction. The one-dimensional case has no $\hat{k}$ dependence so there is no angular expansion nor is a discontinuity correction required.

	3D	2D	1D
Defect type: (dimensionality)	point (0D)	dislocation, crack tip (1D)	Free-surface, boundary (2D)
Brillouin-zone integration:	full BZ	plane(s) $\perp$ to threading direction	line(s) $\perp$ to surface plane
Angular expansion in Brillouin zone:	spherical harmonics $Y_{lm}(\theta_k,\phi_k)$	Fourier series in plane $e^{in\phi_k}$	N/A
Large R elastic Green function:	R^{-1}	$-\ln R+R^0$	R
Large R discontinuity correction:	R^{-3}	R^{-2}	N/A

A. 3D lattice Green function: 0D defects

To facilitate inverse Fourier transformation, the reciprocal-space elastic Green function $\tilde{G}^E$ [Eq. (5)] and discontinuity correction $\tilde{G}^{\mathrm{dc}}$ [Eq. (6)] are expanded as a spherical harmonic series whose coefficients are computed numerically. The expansions

$$\tilde{G}^E(\vec{k})=\frac{1}{k^2}\sum_{l=0}^{L_{\max}}\sum_{m=-l}^{l}\tilde{G}^E_{lm}Y_{lm}(\hat{k}),\quad \tilde{G}^{\mathrm{dc}}(\vec{k})=\sum_{l=0}^{L_{\max}}\sum_{m=-l}^{l}\tilde{G}^{\mathrm{dc}}_{lm}Y_{lm}(\hat{k}),$$

are truncated for $l>L_{\max}$. Both $\tilde{G}^E$ and $\tilde{G}^{\mathrm{dc}}$ are symmetric with respect to inversion, and only even l values are nonzero. The choice of normalized spherical harmonics is given by

$$Y_{lm}(\theta,\phi)=e^{im\phi}\sqrt{\frac{2l+1}{4\pi}\frac{(l-m)!}{(l+m)!}}P_l^m(\cos\,\theta),$$

for $\hat{k}=(\sin\,\theta\cos\,\phi,\sin\,\theta\sin\,\phi,\cos\,\theta)$, where $P_l^m(x)$ is the associated Legendre polynomial without the $(-1)^m$ phase.[34]

Given the spherical harmonic series, inverse Fourier transformation is reduced to a single integral over a finite range. The inverse Fourier transform integral in spherical harmonics over the BZ gives

$$\underline{G}^E(\vec{R})=\sum_{lm}^{L_{\max}}\tilde{G}^E_{lm}Y_{lm}(\hat{R})(-1)^{l/2}\frac{V}{4\pi R}f_l^{(0)}(k_{\max}R),$$

and

$$\underline{G}^{\mathrm{dc}}(\vec{R})=\sum_{lm}^{L_{\max}}\tilde{G}^{\mathrm{dc}}_{lm}Y_{lm}(\hat{R})(-1)^{l/2}\frac{V}{4\pi R^3}f_l^{(2)}(k_{\max}R),$$

where $f_l^{(0)}(x)$ and $f_l^{(2)}(x)$ are integrals over the cut-off function f_{cut}.[42] As noted in the supporting material, both $f_l^{(0)}(x)$ and $f_l^{(2)}(x)$ approach finite values as $x\to\infty$; hence, $\underline{G}^E\sim R^{-1}$ and $\underline{G}^{\mathrm{dc}}\sim R^{-3}$ for large R. Moreover, $f_l^{(0)}(x)\sim x^{1+l}$ and $f_0^{(2)}(x)\sim x^{3+l}$ for small x so the scaling with distance holds also at $R=0$, with $1/k_{\max}$ as the length scale. These results are summarized in Table II.

The inverse Fourier transform of the semicontinuum function $\tilde{G}^{\mathrm{sc}}$ is performed via a discrete transform on a grid in the Brillouin zone. There are different techniques for constructing a k-point mesh[35,36] but a uniform grid of $\vec{k}$ points centered at the gamma point inside the BZ suffices. The primary requirement is that each k point lies in the first BZ so that the points given by $|k|<k_{\max}$ form a sphere. The spacing of the grid is determined by the largest magnitude lattice vector $R_{\max}$ in the desired domain of $\underline{G}^L(\vec{R})$. To avoid aliasing errors, the grid spacing Δk must be smaller than $2\pi/R_{\max}$, although a smaller spacing is preferable. For large R, substituting the elastic Green function for the lattice Green function introduces only small errors, hence reduces the effective $R_{\max}$ and k-point mesh that were used. The deviation is estimated in detail in Sec. IV.

B. 2D lattice Green function: 1D defects

The introduction of a threading direction reduces the lattice Green function to lattice points in a two-dimensional "slab" and modifies the inverse Fourier transformations. The forces and displacements of atoms around a dislocation line or a crack tip have a periodicity given by a threading lattice vector $\vec{t}$. The periodicity is represented in the lattice Green function by the 2D lattice Green function, $\Sigma_n\underline{G}^L(\vec{R}+n\vec{t})$. As with the 3D lattice Green function, evaluation of the 2D lattice Green function is best performed in Fourier space and inverse Fourier transforming to real space. Then,

$$\underline{G}^{L\text{-}2\mathrm{D}}(\vec{R})=\sum_{n=-\infty}^{\infty}\underline{G}^{L\text{-}3\mathrm{D}}(\vec{R}+n\vec{t})$$
$$=\sum_{n=-\infty}^{\infty}\frac{V}{(2\pi)^3}\int\int_{\mathrm{BZ}}\int d^3k e^{-i\vec{k}\cdot\vec{R}}e^{-in\vec{k}\cdot\vec{t}}\tilde{G}^L(\vec{k}).$$

The infinite summation over n gives a delta function on $\exp(i\vec{k}\cdot\vec{t})-1$; when evaluated inside the integral, it produces $(2\pi)/|\vec{t}|$ and restricts the integration to planes in the BZ that are perpendicular to $\vec{t}$; hence,

$$\underline{G}^{L\text{-}2\mathrm{D}}(\vec{R})=\sum_{\vec{k}_\parallel\in\mathrm{BZ}}\frac{V}{|\vec{t}|}\int\int_{\mathrm{BZ}}\frac{d^2k_\perp}{(2\pi)^2}e^{-i(\vec{k}_\perp+\vec{k}_\parallel)\cdot\vec{R}}\tilde{G}^L(\vec{k}_\perp+\vec{k}_\parallel),\quad(9)$$

TABLE II. Summary of equations for lattice Green function computation for different dimensionality. The split of the lattice Green function into three pieces is given for each, along with the angular expansion. The lattice Green function in real space, the limit of large R, and value at $R=0$ are also given. The cut-off function f_{cut} and parameter α are defined in Eq. (7); $k_{\max}$ is the radius of a sphere inscribed in the BZ. All $\vec{k}$ are restricted to be inside the first BZ. The finite BZ summations are done over a grid of N_{kpt} points. The function $\Delta(x)$ is one for $x=0$ and zero elsewhere. The integrals over the cut-off function in 3D $f_l^{(0)}(x)$ and $f_l^{(2)}(x)$, and 2D $F_n^{(0)}(x)$ and $F_n^{(2)}(x)$ are defined in the supporting material (Ref. 42). For the 2D case, the periodicity is defined by a threading lattice vector $\vec{t}$ and $R_\perp$ is the magnitude of $\vec{R}$ perpendicular to $\vec{t}$. In the 1D case, the periodicity is defined by two nonparallel lattice vectors $\vec{t}_1$ and $\vec{t}_2$; $R_\perp$ is the magnitude of $\vec{R}$ perpendicular to the plane of $\vec{t}_1$ and $\vec{t}_2$.

3D:

$$\tilde{G}^{\text{E}}(\vec{k})=\frac{1}{k^2}\sum_{l\ \text{even}}^{L_{\max}}\sum_{m=-l}^{l}\tilde{G}^{\text{E}}_{lm}Y_{lm}(\hat{k}),\quad \tilde{G}^{\text{dc}}(\vec{k})=\sum_{l\ \text{even}}^{L_{\max}}\sum_{m=-l}^{l}\tilde{G}^{\text{dc}}_{lm}Y_{lm}(\hat{k}),\quad \tilde{G}^{\text{sc}}(\vec{k})=[\tilde{D}(\vec{k})]^{-1}-(\tilde{G}^{\text{E}}(\vec{k})+\tilde{G}^{\text{dc}}(\vec{k}))f_{\text{cut}}(k/k_{\max})$$

$$G^L(\vec{R})=\frac{V}{4\pi}\sum_{lm}^{L_{\max}}(-1)^{l/2}\left[\frac{1}{R}\tilde{G}^{\text{E}}_{lm}f_l^{(0)}(k_{\max}R)+\frac{1}{R^3}\tilde{G}^{\text{dc}}_{lm}f_l^{(2)}(k_{\max}R)\right]Y_{lm}(\hat{R})+\frac{1}{N_{\text{kpt}}}\sum_{\vec{k}\in\text{BZ}}e^{-i\vec{k}\cdot\vec{R}}\tilde{G}^{\text{sc}}(\vec{k})$$

$$G^L(\vec{R}\to\infty)=\frac{V}{4\pi}\sum_{lm}^{L_{\max}}(-1)^{l/2}\left[\frac{1}{R}\tilde{G}^{\text{E}}_{lm}+\frac{l(l+1)}{R^3}\tilde{G}^{\text{dc}}_{lm}\right]\left(\frac{\prod_{k\ \text{odd}}^{l}k}{\prod_{k\ \text{even}}^{l}k}\right)Y_{lm}(\hat{R})+O(R^{-5})$$

$$G^L(\vec{R}=0)=\tilde{G}^{\text{E}}_{00}\frac{Vk_{\max}}{2\pi^2}\left[1-\frac{1-\alpha}{2}\right]+\tilde{G}^{\text{dc}}_{00}\frac{Vk_{\max}^3}{2\pi^2}\left[\frac{1}{3}-\frac{(1-\alpha)(2\alpha^2+5\alpha+8)}{30}\right]+\frac{1}{N_{\text{kpt}}}\sum_{\vec{k}\in\text{BZ}}\tilde{G}^{\text{sc}}(\vec{k})$$

2D:

$$\tilde{G}^{\text{E}}(\vec{k}_\perp)=\frac{1}{k_\perp^2}\sum_{n\ \text{even}}^{N_{\max}}\tilde{G}^{\text{E}}_n e^{in\phi_k},\quad \tilde{G}^{\text{dc}}(\vec{k}_\perp)=\sum_{n\ \text{even}}^{N_{\max}}\tilde{G}^{\text{dc}}_n e^{in\phi_k},\quad \tilde{G}^{\text{sc}}(\vec{k})=[\tilde{D}(\vec{k})]^{-1}-(\tilde{G}^{\text{E}}(\vec{k})+\tilde{G}^{\text{dc}}(\vec{k}))f_{\text{cut}}(k/k_{\max})\Delta(\vec{k}\cdot\vec{t})$$

$$G^{\text{L}}(\vec{R})=\frac{V}{2\pi|\vec{t}|}\sum_{n\ \text{even}}^{N_{\max}}(-1)^{n/2}\left[\tilde{G}^{\text{E}}_n F_n^{(0)}(k_{\max}R_\perp)+\frac{1}{R_\perp^2}\tilde{G}^{\text{dc}}_n F_n^{(2)}(k_{\max}R_\perp)\right]e^{in\phi_R}+\frac{1}{N_{\text{kpt}}}\sum_{\vec{k}_\parallel+\vec{k}_\perp\in\text{BZ}}e^{-i(\vec{k}_\parallel+\vec{k}_\perp)\cdot\vec{R}}\tilde{G}^{\text{sc}}(\vec{k}_\parallel+\vec{k}_\perp)$$

$$G^{\text{L}}(R_\perp\to\infty)=\frac{V}{2\pi|\vec{t}|}\left[-\tilde{G}^{\text{E}}_0\ln R_\perp+\sum_{n=2}^{N_{\max}}(-1)^{n/2}\left(\frac{1}{n}\tilde{G}^{\text{E}}_n+\frac{n}{R_\perp^2}\tilde{G}^{\text{dc}}_n\right)e^{in\phi_R}\right]+O(R_\perp^{-4})$$

$$G^{\text{L}}(R_\perp=0)=\tilde{G}^{\text{E}}_0\frac{V}{2\pi|\vec{t}|}\left[\ln(k_{\max})+[\gamma-\ln 2]+\frac{6\alpha^2(3-\alpha)\ln\alpha-(1-\alpha)(5\alpha^2-22\alpha+5)}{6(1-\alpha)^3}\right]+\tilde{G}^{\text{dc}}_0\frac{Vk_{\max}^2}{2\pi|\vec{t}|}\left[\frac{1}{2}-\frac{(1-\alpha)(3\alpha+7)}{20}\right]$$
$$+\frac{1}{N_{\text{kpt}}}\sum_{\vec{k}_\parallel+\vec{k}_\perp\in\text{BZ}}e^{-i\vec{k}_\parallel\cdot\vec{R}}\tilde{G}^{\text{sc}}(\vec{k}_\parallel+\vec{k}_\perp)$$

1D:

$$\tilde{G}^{\text{E}}(\vec{k}_\perp)=\frac{1}{k_\perp^2}\tilde{G}^{\text{E}},\quad \tilde{G}^{\text{dc}}(\vec{k}_\perp)=0,\quad \tilde{G}^{\text{sc}}(\vec{k})=[\tilde{D}(\vec{k})]^{-1}-\tilde{G}^{\text{E}}(\vec{k})f_{\text{cut}}(k/k_{\max})\Delta(\vec{k}\cdot\vec{t}_1)\Delta(\vec{k}\cdot\vec{t}_2)$$

$$G^{\text{L}}(\vec{R})=\frac{V}{|\vec{t}_1\times\vec{t}_2|}\tilde{G}^{\text{E}}\left[-\frac{|R_\perp|}{\pi}\text{Si}(k_{\max}R_\perp)-\frac{\cos(k_{\max}R_\perp)}{\pi k_{\max}}+\int_{\alpha k_{\max}}^{k_{\max}}dk\frac{\cos(kR_\perp)}{\pi k^2}(f_{\text{cut}}(k/k_{\max})-1)\right]$$
$$+\frac{1}{N_{\text{kpt}}}\sum_{\vec{k}_\parallel+\vec{k}_\perp\in\text{BZ}}e^{-i(\vec{k}_\parallel+\vec{k}_\perp)\cdot\vec{R}}\tilde{G}^{\text{sc}}(\vec{k}_\parallel+\vec{k}_\perp)$$

$$G^{\text{L}}(R_\perp\to\infty)=-\frac{1}{2}|R_\perp|\frac{V\tilde{G}^{\text{E}}}{|\vec{t}_1\times\vec{t}_2|}+O(R_\perp^{-1})$$

$$G^{\text{L}}(R_\perp=0)=\frac{V\tilde{G}^{\text{E}}}{|\vec{t}_1\times\vec{t}_2|}\frac{3(-1+\alpha^2-2\alpha\ln\alpha)}{\pi k_{\max}(1-\alpha)^3}+\frac{1}{N_{\text{kpt}}}\sum_{\vec{k}_\parallel+\vec{k}_\perp\in\text{BZ}}e^{-i\vec{k}_\parallel\cdot\vec{R}}\tilde{G}^{\text{sc}}(\vec{k}_\parallel+\vec{k}_\perp)$$

where the (finite) summation is over $\vec{k}_\parallel=m\cdot 2\pi\vec{t}/|\vec{t}|^2$ (m integer) inside the BZ and two-dimensional integration is over $\vec{k}_\perp$ inside the BZ perpendicular to $\vec{t}$. Equation (9) still has a pole in $\tilde{G}^L$ to contend with but it lies purely in the plane of $\vec{k}_\parallel=\mathbf{0}$. Hence, for $\vec{k}_\parallel\neq\mathbf{0}$, the value of $\tilde{G}^L=[\tilde{D}]^{-1}$ is used and a discrete inverse Fourier transform is performed. Then, the remaining difficulty is the $1/k_\perp^2$ pole at the gamma point in the 2D inverse Fourier transform.

The 2D lattice Green function is split into three contributions for inverse Fourier transformation: elastic Green function, discontinuity correction, and semicontinuum function. The elastic Green function $\tilde{G}^E$ and discontinuity correction $\tilde{G}^{\mathrm{dc}}$ are expanded as a truncated Fourier series in the plane of $\vec{k}_\perp$,

$$\tilde{G}^E(\vec{k}_\perp) = \frac{1}{k_\perp^2} \sum_{n=-N_{\max}}^{N_{\max}} \tilde{G}_n^E e^{in\phi_k}, \quad \tilde{G}^{\mathrm{dc}}(\vec{k}_\perp) = \sum_{n=-N_{\max}}^{N_{\max}} \tilde{G}_n^{\mathrm{dc}} e^{in\phi_k},$$

where ϕ_k is the angle of $\vec{k}_\perp$ relative to an (arbitrary) in-plane reference direction $\vec{n}_\perp$ ($\vec{n}_\perp \cdot \vec{t}=0$). Both $\tilde{G}^E$ and $\tilde{G}^{\mathrm{dc}}$ have inversion symmetry so only even n values are nonzero. Note that $\tilde{G}^E(\vec{k})$ and $\tilde{G}^{\mathrm{dc}}(\vec{k})$ are the same functions that appear in the 3D lattice Green function [given by Eqs. (5) and (6)]; for the 2D lattice Green function, they are only evaluated in the plane through the gamma point.

Given the Fourier series, inverse Fourier transformation reduces to a single integral over a finite range. The $\vec{k}_\parallel \neq \mathbf{0}$ terms of Eq. (9) have no singularities so they can be evaluated numerically using a discrete inverse Fourier transform with a discrete grid for $\vec{k}_\perp$, where construction of this grid is described below. Hence, the elastic Green function and discontinuity corrections are only evaluated for $\vec{k}_\parallel = \mathbf{0}$. In the plane, our polar coordinates are $R_\perp = \sqrt{R^2 - (\vec{R}\cdot\vec{t})^2/t^2}$, which is the magnitude of $\vec{R}$ perpendicular to $\vec{t}$, and ϕ_R, which is the in-plane angle of $\vec{R}$ relative to $\vec{n}_\perp$ [$\phi_R = \arccos[(\vec{n}_\perp \cdot \vec{R})/R_\perp n_\perp]$]. Then the inverse Fourier transform integral over the BZ is

$$G^E(\vec{R}) = \sum_{n=-N_{\max}}^{N_{\max}} \tilde{G}_n^E e^{in\phi_R} (-1)^{n/2} \frac{V}{|\vec{t}| 2\pi} F_n^{(0)}(k_{\max} R_\perp),$$

and

$$G^{\mathrm{dc}}(\vec{R}) = \sum_{n=-N_{\max}}^{N_{\max}} \tilde{G}_n^{\mathrm{dc}} e^{in\phi_R} (-1)^{n/2} \frac{V}{|\vec{t}| 2\pi R_\perp^2} F_n^{(2)}(k_{\max} R_\perp),$$

where $F_n^{(0)}(x)$ and $F_n^{(2)}(x)$ are integrals over the cut-off function f_{cut}.[42] As noted in the supporting material, both $F_n^{(0)}(x)$ and $F_l^{(2)}(x)$ approach finite values as $x \to \infty$; hence, $G^E \sim R_\perp^0$ and $G^{\mathrm{dc}} \sim R_\perp^{-2}$ for large $R_\perp$. Moreover, $F_n^{(0)}(x) \sim x^n$ and $F_n^{(2)}(x) \sim x^{2+n}$ for small x; the corresponding limit for $F_0^{(0)}$ gives $\ln k_{\max}$. As a final note, the $n=0$ function goes as $\ln(R_\perp)$ for large $R_\perp$, recovering the well-known result that the isotropic elastic Green function is logarithmic in distance. These results are summarized in Table II.

The inverse Fourier transform of the semicontinuum function $\tilde{G}^{\mathrm{sc}}$ is performed via a discrete transform on a grid lying on planes in the Brillouin zone. The planes are specified by the threading direction in the lattice $\vec{t}$; to form a planar grid requires two in-plane lattice vectors $\vec{n}_\perp$ and $\vec{m}_\perp$. All three vectors are mutually perpendicular although not normalized. The $N \times M$ grid is the combination of $\vec{k}_\parallel$ and $\vec{k}_\perp$ with

$$\vec{k}(t,n,m) = \frac{2\pi\vec{t}}{|\vec{t}|^2} t + \frac{2\pi\vec{n}_\perp}{|\vec{n}_\perp|^2} \frac{n}{N} + \frac{2\pi\vec{m}_\perp}{|\vec{m}_\perp|^2} \frac{m}{M},$$

where t, n, and m are integers that range over the interior of the BZ. The integers N and M specify the in-plane grid spacing, and must be chosen sufficiently large to remove aliasing effects out to $R_{\max}$. As for the 3D lattice Green function, the deviation between the 2D lattice Green function and 2D elastic Green function decreases with distance, thus requiring the computation of the lattice Green function out to a fixed distance dependent on required accuracy.

C. 1D lattice Green function: 2D defects

The introduction of an infinite surface or boundary reduces the lattice Green function to lattice points in a one-dimensional column and modifies the inverse Fourier transformations. The forces and displacements of atoms away from a boundary—be it a free surface, grain boundary, or interface—have a periodicity given by two nonparallel lattice vectors $\vec{t}_1$ and $\vec{t}_2$ lying in the boundary plane. The periodicity is represented in the lattice Green function by the 1D lattice Green function, $\Sigma_{mn} G^L(\vec{R} + m\vec{t}_1 + n\vec{t}_2)$. As with the 3D and 2D lattice Green functions, evaluation of the 1D lattice Green function is best performed in Fourier space and inverse Fourier transforming to real space. Then,

$$\begin{aligned} G^{L\text{-}1\mathrm{D}}(\vec{R}) &= \sum_{n_1,n_2=-\infty}^{\infty} G^{L\text{-}3\mathrm{D}}(\vec{R} + n_1\vec{t}_1 + n_2\vec{t}_2) \\ &= \sum_{n_1,n_2=-\infty}^{\infty} \frac{V}{(2\pi)^3} \int\int\int_{\mathrm{BZ}} d^3k e^{-i\vec{k}\cdot\vec{R}} e^{-in_1\vec{k}\cdot\vec{t}_1 - in_2\vec{k}\cdot\vec{t}_2} \tilde{G}^L(\vec{k}) \\ &= \sum_{\vec{k}_{\mathrm{plane}} \in \mathrm{BZ}} \frac{V}{|\vec{t}_1 \times \vec{t}_2|} \int_{\mathrm{BZ}} \frac{dk_\perp}{2\pi} e^{-i(\vec{k}_\perp + \vec{k}_{\mathrm{plane}})\cdot\vec{R}} \tilde{G}^L(\vec{k}_\perp + \vec{k}_{\mathrm{plane}}), \end{aligned} \tag{10}$$

where the (finite) summation is over

$$\vec{k}_{\mathrm{plane}} = 2\pi \frac{(m_1\vec{t}_1 + m_2\vec{t}_2) \times (\vec{t}_1 \times \vec{t}_2)}{|\vec{t}_1 \times \vec{t}_2|^2},$$

(m_1 and m_2 integer) which are inside the BZ, and one-dimensional integration is over $\vec{k}_\perp$ that are parallel to $\vec{t}_1 \times \vec{t}_2$ and is inside the BZ. This is by virtue of the summation over n_1 and n_2, similar to the 2D lattice Green function. Equation (10) still has a pole in $\tilde{G}^L$ to contend with but it lies purely on the line where $\vec{k}_{\mathrm{plane}} = \mathbf{0}$. Hence, for $\vec{k}_{\mathrm{plane}} \neq \mathbf{0}$, the value of $\tilde{G}^L = [\tilde{D}]^{-1}$ is used and a discrete inverse Fourier transform is performed. Then, the remaining difficulty is the $1/k_\perp^2$ pole at the gamma point in the 1D inverse Fourier transform.

The pole at the gamma point in 1D can be split into two contributions for inverse Fourier transformation: elastic Green function and the semicontinuum function. For one-dimensional variation along $\vec{k}_\perp$, the elastic Green function is

$$\tilde{G}^E(\vec{k}_\perp) = \frac{1}{k_\perp^2}\tilde{G}^E,$$

where the factor $\tilde{G}^E = \tilde{\Lambda}^{(2)}(\vec{t}_1 \times \vec{t}_2 / |\vec{t}_1 \times \vec{t}_2|)$ depends on $\vec{t}_1 \times \vec{t}_2$ and there is no remaining discontinuity at the gamma point. Thus, the semicontinuum function no longer vanishes at the gamma point but instead smoothly approaches a constant value. Thus, the only piece to be treated analytically is the $1/k_\perp^2$ pole at the origin.

The inverse Fourier transformation of the elastic Green function requires the evaluation of a single integral. The elastic Green function in real space is

$$\underline{G}^E(\vec{R})[\vec{k}_\parallel = \mathbf{0}] = \frac{V}{|\vec{t}_1 \times \vec{t}_2|}\int_{\mathrm{BZ}} \frac{dk_\perp}{2\pi} e^{-i\vec{k}_\perp \cdot \vec{R}} \tilde{G}^E(\vec{k}_\perp) f_{\mathrm{cut}}(k/k_{\max})$$

$$= \frac{V}{|\vec{t}_1 \times \vec{t}_2|}\tilde{G}^E \int_{-k_{\max}}^{k_{\max}} \frac{dk}{2\pi} e^{-ikR_\perp} k^{-2} f_{\mathrm{cut}}(k/k_{\max}),$$

where $R_\perp$ is the (positive) magnitude of $\vec{R}$ perpendicular to the plane given by $\vec{t}_1$ and $\vec{t}_2$. The integral over the cut-off function is evaluated in the online supporting material.[42] The limiting behavior of $\underline{G}^E \sim |R_\perp|$ from elasticity theory is recovered. These results are summarized in Table II.

The inverse Fourier transform of the semicontinuum function $\tilde{G}^{\mathrm{sc}}$ is performed via a discrete transform on a grid in lines through the Brillouin zone. The grid spacing along the line must be sufficiently small to remove aliasing effects. As with the 3D and 2D lattice Green functions, the deviation between the 1D lattice and elastic Green functions decreases with distance. Thus, the elastic Green function may be substituted at a fixed distance and require the computation of the full lattice Green function for a finite set of points.

IV. ERROR ESTIMATION FOR LGF

Table II shows that as R becomes larger, the lattice Green function asymptotically matches the elastic Green function; this matching provides the basis for an error estimate of the lattice Green function. The elastic Green function can be computed knowing only the elastic constants; in turn, the elastic constants can be computed even for interactions without a fixed cutoff such as density-functional theory. Hence, while the force-constant matrix computational may induce an artificial cutoff, the asymptotic limit of the lattice Green function is known exactly. Then an estimate of the error in the lattice Green function can be determined by estimating the deviation between the elastic Green function and lattice Green function. Surprisingly, an accurate estimate can be obtained using the elastic constants and the force-constant matrix can be obtained from an artificially truncated supercell even if the true force-constant matrix has nonzero elements outside the supercell. Hence, a single approximate computation of the force-constant matrix in a supercell together with the elastic constants provides an estimate of the accuracy of the supercell computation. This is derived in the online supporting material[42] and shown below.

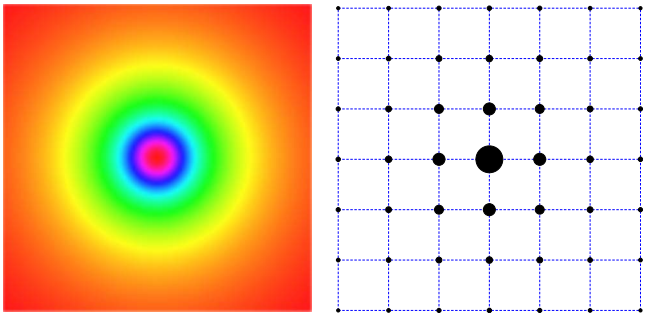

FIG. 2. (Color online) Connection of solution of continuum differential equation mapped onto a lattice equation. The continuum differential equation that defines the solution on the left can be discretized by introducing a grid and approximating derivatives with finite differences over the grid to produce a lattice equation. In the limit that the grid spacing becomes small compared to the length scale of variation of the solution, the discrete approximation matches the continuum solution. This mapping can also be reversed by starting with a grid and a lattice equation, and then taking the limit of zero grid spacing to produce a corresponding continuum differential equation.

A. Derivation

The asymptotic connection between the lattice Green function and the elastic Green function can be understood by viewing the lattice Green function as a "numerical grid" solution to the elastic Green function differential equation, as in Fig. 2. The mapping of a continuum differential equation onto a discrete grid with a lattice equation is a well-known method for the numerical solution of multidimensional partial differential equations.[37] The (partial) derivatives can be approximated using finite differences on the grid. As the grid spacing becomes small compared to the length scale of variation of the solution, the continuum solution is recovered. Moreover, this mapping can be reversed: given a lattice equation, taking the limit of zero grid spacing can recover the continuum partial differential equation. In the case of the lattice Green function, the grid is defined by the crystalline lattice, the lattice equation by Eq. (3), and the corresponding continuum differential equation by Eq. (2).

The analogy of the numerical solution of partial differential equations provides the basic idea for the estimation of the deviation between the lattice Green function and elastic Green function. In finite difference applications, an estimate of the discretization error can be determined by substituting the true continuum solution into the discrete equation and using Taylor series to approximate the deviation.[37] For the lattice Green function equation, it is the elastic Green function that is an approximation but the methodology for error estimation is identical, and provides the deviation between the lattice and elastic Green functions.

The relative deviation of the lattice Green function from the elastic Green function can be extracted using the real-space lattice Green function equation [Eq. (3)]. Define the relative deviation $\underline{\varepsilon}^{\mathrm{GF}}(R)$, for $R > 0$, as

$$\underline{G}^L(\vec{R}) = \underline{G}^E(\vec{R})[\mathbf{1} + \underline{\varepsilon}^{\mathrm{GF}}(R)],$$

and substituting into Eq. (3) for $R > 0$ to get

$$\sum_{\vec{x}} \underline{G}^E(\vec{R}-\vec{x})\underline{D}(\vec{x}) + \sum_{\vec{x}} \underline{G}^E(\vec{R}-\vec{x})\underline{\varepsilon}^{\mathrm{GF}}(\vec{R}-\vec{x})\underline{D}(\vec{x}) = \mathbf{0}.$$

The detailed derivation of an approximate solution for the relative error appears in the supporting material,[42]

$$\underline{\varepsilon}^{\mathrm{GF}}(R) \approx \frac{2V}{R^2}\underline{\delta C}(R)[\underline{D}(\mathbf{0})]^{-1} + \frac{10}{3R^2}\frac{\tilde{G}_{00}^{\mathrm{dc}}(R)}{\tilde{G}_{00}^{E}}, \qquad (11)$$

where $V\underline{\delta C}_{ab}(R) = \Sigma_x x^2 \underline{D}_{ab}(\vec{x}) - \Sigma_{|\vec{x}|\le R} x^2 \underline{D}_{ab}(\vec{x})$ is the error in elastic constants from truncating the force constants at R and $\tilde{G}_{00}^{\mathrm{dc}}(R)$ is the spherically averaged discontinuity correction with a truncated force-constant matrix. The first term dominates when R is small compared to the true range of the interaction ("region 1") and the second term dominates when R becomes comparable to the interaction range ("region 2"). Overall, the relative error estimate scales as R^{-2}. The main feature of Eq. (11) is that the two pieces of the estimate can be determined using a single supercell calculation even if the force-constant matrix lacks a finite interaction cutoff. The cutoff is given by either the size of the supercell in a direct force computation or the inverse q-point grid spacing in a linear-response calculation. For direct force, it is assumed that the effect of folding the force-constant matrix into the supercell is approximately equivalent to truncating it outside the supercell.

B. Numerical example of error estimate: FCC lattice

While Eq. (11) has the advantage of being computable for long-ranged force-constant matrices, it is not clear if too much accuracy has been lost in the series of approximations so a numerical example highlights the range of applicability. A series of pseudorandom long-range force-constant matrices are generated on a face-centered-cubic lattice with characteristics related to real material systems, and for each, the lattice Green function, relative deviation to the elastic Green function, and region 1 and 2 estimates are computed.

The force-constant matrices are generated using $\underline{D}(R) \sim \sin(\pi R/a_0)R^{-4}$, cutoff at $15a_0$ with lattice constant $a_0=1$. The functional form is chosen to provide a long-range interaction whose falloff is still fast enough to produce finite elastic constants in Eq. (1). The $\sin(\pi R/a_0)$ functional form produces a Friedel-like oscillation, as might be expected in a metallic system. The force-constant matrix elements at each site are pseudorandom numbers from a Gaussian distribution with mean of zero and standard deviation $\sin(\pi R/a_0)R^{-4}$. The force-constant matrix is symmetrized using the cubic point group. The elastic constants and phonons are computed; if there are unstable phonons or the elastic anisotropy is greater than three, the force-constant matrix is rejected. 100 random, stable, long-range face-centered-cubic force-constant matrices are generated in this manner; for each, the lattice and elastic Green functions along with the relative deviation are generated. The force-constant matrix is "folded down" into supercells from $2\times2\times2$ to $14\times14\times14$ in order to compute the region 1 and 2 estimates in Eq. (11).

Figure 3 shows the true deviation and estimates from our test case for both a single example and the average results

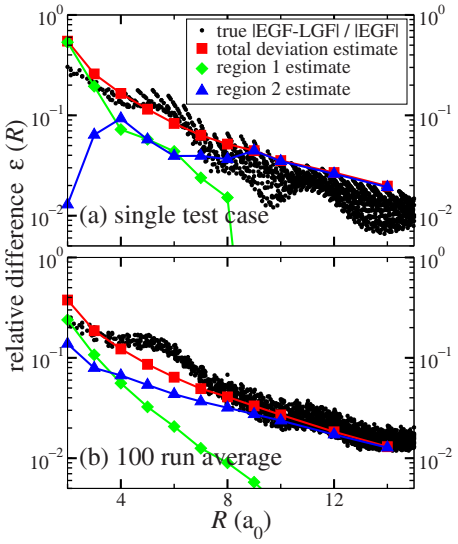

FIG. 3. (Color online) Relative deviation between EGF and LGF for face-centered-cubic test case. The points give the deviation between the lattice Green function, computed with the full force-constant matrix, and the elastic Green function. The region 1 and 2 estimates are computed using the folded force-constant matrix in cubic supercells, and combined, as in Eq. (11), to produce the total deviation estimate. (a) Single random force-constant matrix shows an individual example of error estimation. (b) 100 different random force-constant matrices were computed along with their associated LGFs. The average deviation over the ensemble average shows accurate computation of the error even for the case of small supercells $(2\times2\times2)$ with the long-range force-constant matrix (cutoff at $15a_0$).

from the 100 force-constant matrices. As expected from the derivation, the region 1 estimate dominates for small R and falls off as the supercell becomes large enough to accurately produce the elastic constants. The region 2 estimate becomes important for large R, capturing the long-range effect from the discontinuity correction. What is especially encouraging is that the error estimate is accurate even for small supercells such as $2\times2\times2$, where the supercell force-constant matrix calculation is clearly inaccurate due to the long range. This is perhaps the most impressive feature of Eq. (11): Even when the force-constant matrix calculation comes from a small supercell, the known elastic constants can still provide an accurate error estimate without requiring comparisons to larger supercells. Hence, a supercell-size effect estimate on the lattice Green function computation is provided from a *single* supercell force-constant matrix computation.

V. DISCUSSION

The deviation between the lattice Green function and elastic Green function in Eq. (11) can be described by a single length scale l_{elas} that characterizes the recovery of continuum elastic behavior from atomistic lattice behavior: $\underline{\varepsilon}^{\mathrm{GF}}(R) \approx (l_{\mathrm{elas}}/R)^2$. This length scale determines the range where the lattice Green function should be computed in lieu of the elastic Green function. For example, if the magnitude of the largest lattice vector $R_{\max}$ is greater than $10l_{\mathrm{elas}}$, the lattice

Green function can be computed for lattice vectors $|\vec{R}| < 10l_{\text{elas}}$ and the elastic Green function used for the remainder while introducing a total error of 1%. This choice can greatly speed the computation of the lattice Green function for large simulations by (1) limiting the k-point grid size and (2) restricting the set of points over which the full lattice Green function must be computed.

The length scale l_{elas} is also a fundamental length scale for quasicontinuum[38] and flexible boundary condition methods[13,14] where it determines the range at which the relaxation response using elastic finite elements or the bulk continuum is accurate compared to atomistic response. This length is not necessarily the same as the interaction force cutoff: it may be larger or smaller. For example, the region 2 estimate of deviation for an isotropic nearest-neighbor interaction gives $l_{\text{elas}}=\sqrt{1/6}R_{\text{nn}}\approx 0.4R_{\text{nn}}$, which suggests transitioning from atomistic to finite elements at twice the interaction cutoff produces errors on the order of 4% in position. On the other extreme, density-functional theory calculations in metals have shown surprisingly small l_{elas}, considering the known long-range interactions in metallic systems.[5] It is the small value of l_{elas} that has allowed the accurate calculation of isolated dislocations using flexible boundary-condition methods in density-functional theory. Knowledge of l_{elas} is essential to constructing accurate computational cells that are large enough to produce accurate response but do not waste computational resources treating interactions that can be replaced with elastic response.

This paper presents an accurate computational algorithm for the lattice Green function from limited force-constant matrix information together with the elastic constants. In conjunction, an accurate error estimate using the limited force-constant matrix computable from a single supercell computation allows measurement of the supercell-size effect. The error estimate produces a length scale l_{elas}, which characterizes the crossover from atomistic harmonic response to continuum elastic response. The algorithm for lattice Green function computation together with the determination of crossover length scale has already allowed the accurate computation of single extended dislocation defects using density-functional theory.[5–7,39,40] The approach can also be utilized to implement flexible boundary-condition methods for point defects, crack opening, tip propagation, and surfaces and boundaries coupled with density-functional theory, providing chemically accurate interactions coupled with correct treatment of the long-range elastic response of extended defects.

ACKNOWLEDGMENTS

The author thanks R. Hennig, S. Rao, J. Wilkins, and C. Woodward for helpful discussions. This research was supported by the Air Force Office of Scientific Research. Computational resources were provided by the Ohio Supercomputing Center.

*Present address: Department of Material Science and Engineering, University of Illinois, Urbana-Champaign, 1304 W. Green Street, Urbana, IL 61801, USA. dtrinkle@illinois.edu

[1] P. Haasen, *Physical Metallurgy*, 3rd ed., edited by J. Mordike (Cambridge University Press, Cambridge, 1996).
[2] A. N. Stroh, J. Math. Phys. **41**, 77 (1962).
[3] D. J. Bacon, D. M. Barnett, and R. O. Scattergood, Prog. Mater. Sci. **23**, 51 (1980).
[4] P. Rudolph and M. Jurich, J. Cryst. Growth **198-199**, 325 (1999).
[5] C. Woodward and S. I. Rao, Philos. Mag. A **81**, 1305 (2001).
[6] C. Woodward and S. I. Rao, Phys. Rev. Lett. **88**, 216402 (2002).
[7] C. Woodward and S. I. Rao, Philos. Mag. **84**, 401 (2004).
[8] T. A. Arias and J. D. Joannopoulos, Phys. Rev. Lett. **73**, 680 (1994).
[9] S. L. Frederiksen and K. W. Jacobsen, Philos. Mag. **83**, 365 (2003).
[10] J. R. K. Bigger, D. A. McInnes, A. P. Sutton, M. C. Payne, I. Stich, R. D. King-Smith, D. M. Bird, and L. J. Clarke, Phys. Rev. Lett. **69**, 2224 (1992).
[11] S. Ismail-Beigi and T. A. Arias, Phys. Rev. Lett. **84**, 1499 (2000).
[12] J. E. Sinclair, P. C. Gehlen, R. G. Hoagland, and J. P. Hirth, J. Appl. Phys. **49**, 3890 (1978).
[13] R. Thomson, S. J. Zhou, A. E. Carlsson, and V. K. Tewary, Phys. Rev. B **46**, 10613 (1992).
[14] S. Rao, C. Hernandez, J. P. Simmons, T. A. Parthasarathy, and C. Woodward, Philos. Mag. A **77**, 231 (1998).
[15] C. Woodward, Mater. Sci. Eng., A **400-401**, 59 (2005).
[16] L. M. Canel, A. E. Carlsson, and R. Thomson, Phys. Rev. B **52**, 158 (1995).
[17] S. I. Rao and C. Woodward, Philos. Mag. A **81**, 1317 (2001).
[18] L. H. Yang, P. Söderlind, and J. A. Moriarty, Philos. Mag. A **81**, 1355 (2001).
[19] S. Rao, T. A. Parthasarathy, and C. Woodward, Philos. Mag. A **79**, 1167 (1999).
[20] V. K. Tewary, Phys. Rev. B **69**, 094109 (2004).
[21] M. Ortiz and R. Phillips, Adv. Appl. Mech. **36**, 1 (1999).
[22] V. K. Tewary, Adv. Phys. **22**, 757 (1973).
[23] I. R. MacGillivray and C. A. Sholl, J. Phys. F: Met. Phys. **13**, 23 (1983).
[24] K. Kunc and R. M. Martin, Phys. Rev. Lett. **48**, 406 (1982).
[25] S. Wei and M. Y. Chou, Phys. Rev. Lett. **69**, 2799 (1992).
[26] W. Frank, C. Elsässer, and M. Fähnle, Phys. Rev. Lett. **74**, 1791 (1995).
[27] K. Parlinski, Z-.Q. Li, and Y. Kawazoe, Phys. Rev. Lett. **78**, 4063 (1997).
[28] S. Baroni, P. Giannozzi, and A. Testa, Phys. Rev. Lett. **58**, 1861 (1987).
[29] A. A. Quong and B. M. Klein, Phys. Rev. B **46**, 10734 (1992).
[30] M. Born and K. Huang, *Dynamical Theory of Crystal Lattices* (Oxford University Press, London, 1954).
[31] A. A. Maradudin, E. W. Montroll, and G. H. Weiss, *Theory of Lattice Dynamics in the Harmonic Approximation*, Solid State Physics Suppl. 3, 2nd ed. (Academic, New York, 1971).
[32] N. W. Ashcroft and N. D. Mermin, *Solid State Physics* (Saun-

ders, Philadelphia, 1976).
[33] V. K. Tewary and R. Bullough, J. Phys. F: Met. Phys. **1**, 554 (1971).
[34] M. Abramowitz and I. A. Stegun, *Handbook of Mathematical Functions*, Applied Mathematics Series (National Bureau of Standards, Washington, 1964), Vol. 55.
[35] D. J. Chadi and M. L. Cohen, Phys. Rev. B **8**, 5747 (1973).
[36] H. J. Monkhorst and J. D. Pack, Phys. Rev. B **13**, 5188 (1976).
[37] R. D. Richtmyer and K. W. Morton, *Difference Methods for Initial Value Problems*, 2nd ed. (Wiley, New York, 1967).
[38] R. E. Rudd and J. Q. Broughton, Phys. Rev. B **72**, 144104 (2005).
[39] D. R. Trinkle and C. Woodward, Science **310**, 1665 (2005).
[40] C. Woodward, D. R. Trinkle, L. G. Hector, and D. L. Olmsted, Phys. Rev. Lett. **100**, 045507 (2008).
[41] See (Ref. 30) for a discussion of phonons in ionic crystals.
[42] See EPAPS Document No. E-PRBMDO-78-057825 for the derivation of the analytic inverse Fourier transform expressions in 3D, 2D, and 1D; expressions using alternative cut-off functions; and the detailed derivation of the lattice Green function error estimate. For more information on EPAPS, see http://www.aip.org/pubservs/epaps.html.